# A Novel Dual CC–CV Output Wireless EV Charger With Minimal Dependency on Both Coil Coupling and Load Variation

Subhranil Barman* and Kishore Chatterjee†
Indian Institute of Technology Bombay
Powai, Maharashtra - 400076
Mumbai, India
Email: subhrabarman@ee.iitb.ac.in*; kishore@iitb.ac.in†

## Keywords

≪Electric Vehicle≫, ≪Battery charger≫, ≪Wireless power transmission≫, ≪Power converters for EV≫, ≪Compensation≫

## Abstract

Robust and efficient wireless EV charging requires load and coupling independent CC and CV modes. Existing literature focus either on CC or CV mode. The characteristics of the schemes which cater to both the modes are affected by load and coupling coefficient. In this paper, an improved dual output charger topology is proposed that is maximally independent from variations in coil coupling and load. Relevant analysis and simulation results are shown to validate the working of the proposed topology.

## Introduction

Moving forward, electric vehicles (EVs) are the way ahead for transportation. A key aspect in the development of EVs is the charging of their batteries. The most commonly used batteries in EVs are Lithium-ion (Li-ion) batteries. As they cannot withstand overvoltage, provision of the two standardised charging modes, constant current (CC) and constant voltage (CV), in an appropriate sequence is crucial [1], with smooth transition between them. This feature should be catered by wireless battery chargers (WBCs) in an efficient and robust manner, along with fulfilling other requisite characteristics.

WBCs generally employ inductive power transfer (IPT) using magnetically coupled coils, wherein the power transfer occurs in "non-radiative" form. The basic components of inductive WBCs are: isolated bridge converters, compensation circuits and optionally DC backend converters. The bridge converters usually involve single active bridges (SAB) for unidirectional power flow, or dual active bridges (DAB) for bidirectional power flow. Although WBCs provide contactless charging, their operation is dependent on the alignment between the transmitter and the receiver coils. For "true wireless" systems, the alignment between the aforesaid coils depends on factors such as ground level conditions, tire pressure, parking manoeuvres, etc. The change in the coupling coefficient of the two coils affects power transfer, output characteristics, operating frequency, and several other parameters. Coupling and load conditions also govern the charger operation in zero phase angle (ZPA) condition. Further, the cascade network consisting of inverter, coupled coils and rectifier reduces the overall efficiency. In view of these aspects, an ideal WBC should have the following features - (1) maximal operational independence from variations of both coil coupling and load, (2) minimized size and components, (3) ZPA operation with soft switching, and (4) maximum efficiency in both CC and CV modes [2].

The aforementioned features can be achieved by employing (1) appropriate modifications in the inversion and/or rectification stages, (2) DC front-end or back-end converters, (3) modified compensation circuits with or without additional switches, or (4) frequency or phase modulation. Literature survey in this regard reveals the following significant aspects. (1) A WBC configuration with a fully controlled input side

inverter and a output diode rectifier is preferable to minimize component count and simplify the control at the vehicular end. (2) DC converters provide independent output regulation, but have extra switches, additional DC side magnetics, lower efficiency etc., which have led to their elimination with advanced topologies. (3) Extensive techniques that are reported in [1]– [4] are not fully sufficient, as they have either inherent CC output, or CV output with partial or no ZPA, and/or are operated at frequencies dependent on coupling coefficient, $k$. Besides this, topological modifications involving switched compensation networks [5], [6], wherein the compensation circuit is altered by applying appropriate switching states, have several drawbacks like - charge modes being dependent on $k$, higher component count, lower efficiency ($\eta$), etc. (4) Moreover, soft control methods involving frequency modulation and phase shift control can only partially fulfill the required specifications, and have poor wide load range operation and high complexity.

To improve upon all these aspects, a compensation strategy incorporating multiple and multi-resonant LC tanks has been proposed in this paper to achieve a re-configurable charger which can provide both CC and CV modes of operation. The proposed modifications have been targeted in the compensation section as it affects several parameters such as ZPA, output characteristics, power transfer capability, size, etc. Analysis and methods followed for the development of the proposed charging topology, as well as their features and benefits, are presented, along with the future scope of the topology. The salient features of the proposed topology are as follows : (1) it does not require additional switches to realize distinct compensation networks for both CC and CV modes; (2) it eliminates the dependency of operating frequencies from coil coupling; (3) constant output current and voltage are obtained during CC and CV modes respectively; (4) load and coupling coefficient independent ZPA is achieved in both the modes, thus fulfilling all desired features.

## Passive Network Analysis

For obtaining both CC and CV modes from a single input source, different circuits are required. To achieve that, a single topology may be modified to have different structures, however, additional switches are undesirable. Hence, a passive network analysis is presented here as per [7] that describes the basic principle of obtaining constant current or voltage outputs from any given input source, which is - allocation of suitable passive networks between source and load. Accordingly, the requisite modifications for developing a dual output topology devoid of any additional switches are shown.

The passive networks required for obtaining load independent CC output from a voltage source, and CV output from a current source, are shown [7] in Fig. 1. There can be several combinations of $z_a, z_b$ and $z_c$ [7]. The CC and CV output expressions are also given. Similar networks can be derived for other possible combinations of input and output configurations [7]. Based on this principle, it is evident that the CC and CV modes require different network configurations. Hence, to implement them, resonance is used for reconfiguring the topology without utilizing any switches. Since in a single passive network stage, tunable parameters are less for the provision of ZPA independent of load resistance $R_0$ and coil coupling coefficient $k$ [7], multiple network stages are employed with appropriate resonating conditions.


Fig. 1: Circuits for (a) CC output from a voltage source, and (b) CV output from a current source

$$\text{CC ouput from voltage source } i_o = \frac{u_i}{z_a} = \frac{u_i}{z_b}; \quad \text{CV output from current source } u_o = z_a i_i = z_b i_i \quad (1)$$

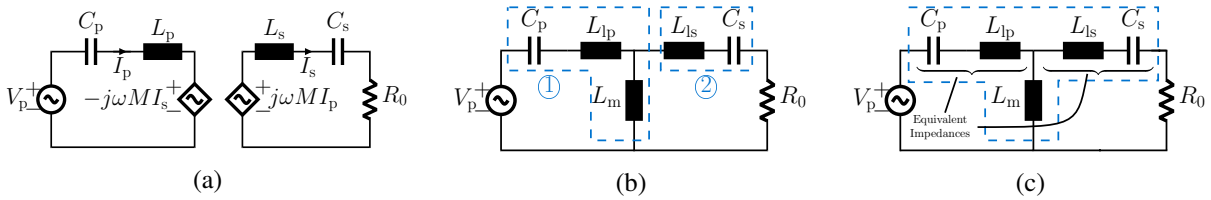


Fig. 2: (a) SS topology, and its constituent network stages for (b) CC mode (c) CV mode

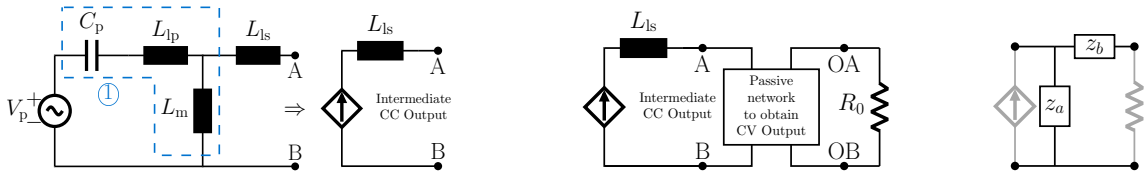


Fig. 3: (a), (b) Secondary side with intermediate current source ; (c) Network VC-LC/CL

## Synthesis of the Proposed Topology

As a starting point, the existing series-series (SS) topology is chosen as a base circuit as it already provides CC mode with ZPA and has very few passive components [1]. This is subsequently modified to implement the CV mode of operation. The configuration of the SS topology is shown in Fig. 2a. As can be seen in Fig. 2, the CC mode circuit can be decomposed into passive network blocks [7] based on the input type - a voltage source, and output type - constant current. There are two cascaded stages in Fig. 2b - ① network CV-CL (nomenclature - 'C' : CC output, 'V' : voltage source input, 'C' : capacitor $C_p$, impedance as seen from the network input, 'L' - next impedance encountered - formed by $L_{lp}$ and $L_m$), and ② $L_{ls}$ and $C_s$ which form a series impedance. Stage ① generates an intermediate CC output, which is then reflected to load $R_0$ via stage ②. Similar analysis for CV mode yields network type VV-xLx (Fig. 2c) - where 'x' signifies that the combination of $C_p, L_{lp}$, and $C_s, L_{ls}$ are treated as equivalent inductors or capacitors. A single network stage is present in this case. In CC mode, as there are two stages, $Z_p$ is independent of $R_0$ - the second stage facilitates tuning. In CV mode, $Z_p$ becomes $R_0$ dependent, as the single stage does not present adequate tuning parameters. Besides, $\omega_0 \propto k$ for the CV mode because the resonance condition involves $L_m$ (or $L_{lp}$). Thus it can be inferred that the synthesized topology must consist of multiple network stages for load independent ZPA provision. Also, resonance conditions must involve the entire self inductances of the coils for providing charging modes unaffected by $k$. Besides, for the proposed topology, the CC mode frequency $\omega_{0cc}$ is selected to be lower than the CV mode frequency $\omega_{0cv}$. This is because $R_0$ assumes a low value in the CC mode and increases considerably in the CV mode [3]. To achieve optimal $\eta$ for the entire load range, SS topologies are operated such that $\omega_{0cc} < \omega_{0cv}$ [2, 3]. This can be supported by $\eta$ plots for different frequency ratios.

### Proposed Modifications for Achieving Desired Features

The secondary side structure is shown in Fig. 3. Using the intermediate current source as an input, as per Fig. 1b, a CV output can be obtained by placing network stages VC-CL or VC-LC [7] shown in Fig. 3c between 'A', 'B' and 'OA', 'OB' in Fig. 3b. As per the aforesaid nomenclature, for the network VC-CL, $z_a$ is capacitive and $z_b$ is inductive, and the opposite holds for VC-LC. Here only network VC-CL is feasible, as a contradiction occurs for VC-LC wherein CC and CV mode frequencies become equal. During CV mode, to implement VC-CL, two LC tanks - SLCA and SLCB, are used (as shown in Fig. 4), wherein SLCA forms an inductor $L_{seq}$, while SLCB forms a capacitor $C_{seq}$. During CC mode, SLCA forms a capacitor $C_s$ and SLCB, which must remain disconnected, forms an open circuit. While shifting from $\omega_{0cc}$ to $\omega_{0cv}$, the impedance of SLCA changes from being capacitive to inductive, while it is the opposite for SLCB (open circuit to capacitive). Thus a parallel tank is used for SLCB, and a series tank is used for SLCA. To enable ZPA operation, the primary side needs to resonate during both CC and

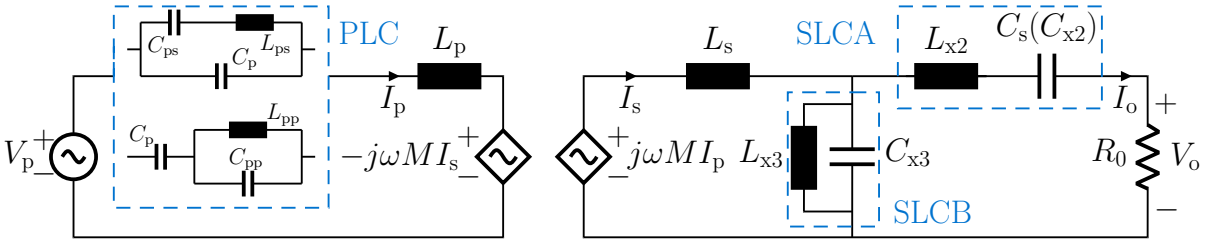


Fig. 4: Proposed topology

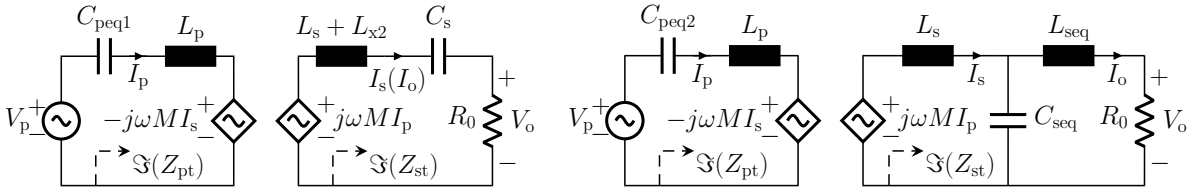


(a) (b)

Fig. 5: Equivalent circuits of the proposed topology for (a) CC mode, and (b) CV mode

CV modes. Hence a multi resonant tank PLC involving capacitor $C_p$ is used instead of just $C_p$ being connected in series with $L_p$, (as is present in the primary of a conventional SS topology), since $C_p$ and $L_p$ can only resonate at one frequency. Two structures are possible in this case - a parallel LC tank in series with $C_p$, or a series LC tank in parallel with $C_p$, both of which are in series with $L_p$. PLC is designed to form $C_{peq1}$ and $C_{peq2}$ in CC and CV modes respectively. Combining the modified primary and secondary circuits, the final proposed topology is shown in Fig. 4.

## Independence of ZPA from $R_0, k$ in Both Modes

To achieve $R_0$ and $k$ independent ZPA, the impedances $\Im(Z_{pt}), \Im(Z_{st})$ in Fig. 5 must be nullified in both modes. For $\Im(Z_{pt})$ and $\Im(Z_{st})$, given in (2) and (3), to be zero at both $\omega_{0cc}$ and $\omega_{0cv}$, such that secondary to primary transferred impedance $Z_{tr}$ is real ($=\frac{\omega^2 M^2}{R_0}$ [8], where $\omega = \omega_{0cc}, \omega_{0cv}$), we get $\omega_{0cc}^2 L_p C_{peq1} = \omega_{0cv}^2 L_p C_{peq2} = 1$, $\omega_{0cc}^2 (L_s + L_{x2}) C_s = 1$ and $\omega_{0cv}^2 L_s C_{seq} = \omega_{0cv}^2 L_{seq} C_{seq} = 1$ (implying $L_{seq} = L_s$).

$$\text{CC Mode}: \quad \Im(Z_{pt}) = \frac{\omega_{0cc}^2 L_p C_{peq1} - 1}{\omega_{0cc} C_{peq1}}, \quad \Im(Z_{st}) = \frac{\omega_{0cc}^2 (L_s + L_{x2}) C_s - 1}{\omega_{0cc} C_s} \tag{2}$$

$$\text{CV Mode}: \quad \Im(Z_{pt}) = \frac{\omega_{0cv}^2 L_p C_{peq2} - 1}{\omega_{0cv} C_{peq2}}, \quad \Im(Z_{st}) = \frac{-R_0(\omega_{0cv}^2 L_s C_{seq} - 1)}{\omega_{0cv} C_s R_0 + j(\omega_{0cv}^2 L_{seq2} C_{seq} - 1)} \tag{3}$$

## Load and Coupling Independent Resonant Frequencies

From (2) and (3), the CC and CV mode resonant frequencies are obtained as given below, which shows that both $\omega_{0cc}$ and $\omega_{0cv}$ (and hence ZPA as well) are independent of $R_0$ and $k$.

$$\omega_{0cc} = \frac{1}{\sqrt{(L_s + L_{x2}) C_{sx2}}} = \frac{1}{L_p C_{peq1}}, \; \omega_{0cv} = \frac{1}{\sqrt{L_{seq} C_{seq}}} = \frac{1}{L_p C_{peq2}} \tag{4}$$

## Dual Output Characteristics

The dual output (CC and CV) characteristics can be derived by circuit analysis of the equivalent figures shown in Fig. 5a and Fig. 5b at the resonant frequencies $\omega_{0cc}$ and $\omega_{0cv}$ respectively. It can be seen that both the outputs are load independent as shown in (5), thereby fulfilling all the required features.

$$\text{CC mode} \rightarrow I_o = \frac{V_p}{\omega_{0cc} M}, \quad \text{CV mode} \rightarrow V_o = \frac{L_s}{M} V_p \tag{5}$$

## Design Considerations for the Proposed Topology

The tanks PLC, SLCA and SLCB are designed as per their required functionality, such that the overall tank impedances are equal to the requisite equivalent impedances, as shown in Table I. For the design of coil parameters $L_p$ and $L_s$, (5) is employed, wherein $M$ is replaced by $k\sqrt{nL_pL_s}$, $n$ being the turns ratio. Using the value of $R_0$ at the transition point between CC to CV mode, given as $R_{crit} = \frac{V_o}{I_o} = \frac{8}{\pi^2}(\frac{V_{Bat}}{I_{Bat}})$, we can get $L_s$ and $L_p$. If $L_p = nL_s$ is chosen, then $V_p = kV_o$, where $V_p$ has to be regulated if $k$ varies; otherwise $L_p \propto \frac{nL_s}{k^2}$, wherein $L_p$ has to be adjusted with variations in $k$. For this topology, the design approach keeping $L_p = nL_s$ is chosen. The coil and tank parameters are shown in Table II. Here, $\sigma_\omega > 1$ and $\omega_{0cc} < \omega_{0L_pC_p} < \omega_{0cv}$ is required ($\sigma_\omega = \frac{\omega_{0cv}}{\omega_{0cc}}$, and $\omega_{0L_pC_p}$ is the resonant frequency of $L_p$ and $C_p$), which gives a design condition for $\omega_{0L_pC_p}$ as $\omega_{0cv} > \omega_{0cc}$. The frequencies $f_{0cc}$ $(\omega_{0cc}), f_{0cv}$ $(\omega_{0cv})$ and $f_{0L_pC_p}$ $(\omega_{0L_pC_p})$ are chosen as some factors of a base frequency $f_{base}$, such that $f_{0cc} = \beta_\omega f_{base}$, $f_{0cv} = \sigma_\omega f_{0cc}$, and $f_{0L_pC_p} = \lambda_\omega f_{0cc}$. Optimal values of the turns ratio $n$, and the frequency tuning parameters $\beta_\omega, \sigma_\omega$, and $\lambda_\omega$ are selected by analysis of the variation trends of three key aspects, mainly - (a) passive component values, (b) peak stresses of components, and (c) average efficiency $\eta$ for the entire load range.

Table I: Primary and secondary tank design features

| Tank | CC Mode Equivalent Impedance | CV Mode Equivalent Impedance |
|---|---|---|
| PLC | $\frac{-j}{\omega_{0cc}C_{peq1}}$ | $\frac{-j}{\omega_{0cv}C_{peq2}}$ |
| SLCA | $j\omega_{0cc}L_{x2} - \frac{j}{\omega_{0cc}C_{x2}}$ | $j\omega_{0cv}L_{seq}$ |
| SLCB | $\infty$ (open circuit) | $\frac{-j}{\omega_{0cv}C_{seq}}$ |

Table II: Significant parameters of the proposed topology

| | | | |
|---|---|---|---|
| $L_s = \frac{R_{crit}}{\omega_{0cc}}$ | $L_p = nL_s$ | $f_{0cc} = \beta_\omega f_{base},\ f_{0L_pC_p} = \lambda_\omega f_{0cc},\ f_{0cv} = \sigma_\omega f_{0cc}$ | |
| PLC → ($C_p$ in series with parallel LC tank) | $L_{pp} = \frac{(\omega_{0cv}^2 L_pC_p - 1)(1-\omega_{0cc}^2 L_pC_p)}{(\omega_{0cc}^2 C_p)(\omega_{0cv}^2 L_pC_p)}$<br>$C_{pp} = \frac{C_p}{(\omega_{0cv}^2 L_pC_p - 1)(1-\omega_{0cc}^2 L_pC_p)}$ | PLC → ($C_p$ in parallel with series LC tank) | $L_{ps} = \frac{L_p}{(\omega_{0cv}^2 L_pC_p - 1)(1-\omega_{0cc}^2 L_pC_p)}$<br>$C_{ps} = \frac{(\omega_{0cv}^2 L_pC_p - 1)(1-\omega_{0cc}^2 L_pC_p)}{(\omega_{0cc}^2 L_p)(\omega_{0cv}^2 L_pC_p)}$ |
| $C_p$ (for both forms of PLC) = $\frac{1}{\omega_{0L_pC_p}^2 L_p}$ | | | |
| SLCA → $L_{x2} = \frac{\sigma_\omega^2+1}{\sigma_\omega^2-1}L_s,\ C_{x2} = C_s = \frac{\sigma_\omega^2-1}{2\omega_{0cv}^2 L_s}$ | | SLCB → $L_{x3} = \frac{1}{\omega_{0cc}^2 C_{x3}},\ C_{x3} = \frac{\sigma_\omega^2 C_{seq}}{\sigma_\omega^2-1}$ | |

One thing to note is that using (4) and (5), and noting that $C_{sx2} = C_s$ (as $C_{sx2}$ is the capacitor $C_s$ from the base circuit of SS topology), we get (6). For a normal SS topology, with the same $C_s$, and secondary inductance denoted by $L_s'$, the resonant frequency is $\omega' = 1/(L_s'C_s)$, and $|I_s| = (V_p/k)\sqrt{(C_s/L_p)}$. If for the sake of comparison $\omega' = \omega_{0cc}$ is considered, then $I_s$ is increased by a factor $\sqrt{(1+L_{x2}/L_s)}$ in the proposed topology. Alternatively, it can be said that $L_s$ can be reduced for obtaining the same $I_o$ (or $I_s$), as is evident from the expressions of $\omega_{0cc}$ and $\omega'$. If $L_s$ can be reduced, then it not only reduces the coil size on the car side, but also helps reduce $I_p$, because noting that $L_{seq} = L_s$, we get (7). As per (7), the magnitude of $I_p$ throughout the charging process can be quite high as $L_s > M$ by a large extent. $|I_p|$ will vary with load induced variations, but its peak will occur at the starting point of CV mode (or transition point from CC to CV mode) and is obtained by substituting the peak value of $I_o$ during CC mode (a known constant) in (7). Hence $I_p$ can be reduced by lowering the peak value of $I_p$ by adjusting $L_s$ in (7).

$$|I_s| = \frac{V_p}{\omega_{0cc}M} = \frac{V_p}{k}\sqrt{\frac{(L_s+L_{x2})C_s}{L_pL_s}} = \frac{V_p}{k}\sqrt{\frac{C_s}{L_p}}\sqrt{1+\frac{L_{x2}}{L_s}} \tag{6}$$

$$|I_p| = \frac{V_p(L_s+L_{x2})C_{sx2}R_0}{M^2} \text{ during CC mode;} \quad = \frac{L_sI_o}{M} \text{ during CV mode} \tag{7}$$

Table III: Simulation parameters {transition from CC to CV mode : $t = 0.7$ s (after $V_o = V_{Bat}$)}

| | | |
|---|---|---|
| $V_{Bat} = 300$ V | $I_{Bat} = 10$ A | $R_{Bat} = 30\ \Omega$, $R_{crit} = 24.3\ \Omega$ |
| $L_s = 77.4\ \mu$H | $L_p = 344.1\ \mu$H | $n = 4.44$ |
| $\beta_\omega = 1$, $f_{0cc} = 50$ kHz | $\lambda_\omega = 1.336$, $f_{0L_pC_p} = 66.8$ kHz | $\sigma_\omega = 1.6$, $f_{0cv} = 80$ kHz |
| $L_{pp} = 81.7\ \mu$H, $C_{pp} = 86.4$ nF | $L_{x2} = 176.6\ \mu$H, $C_{x2} = 39.9$ nF | $L_{x3} = 120.7\ \mu$H, $C_{x3} = 83.9$ nF |
| $k = 0.3$, $V_p = 170.8$ V | $k = 0.35$, $V_p = 199.3$ V | |

## Simulated Performance

The proposed topology has been simulated in MATLAB-Simulink (where $C_p$ is in series with a parallel LC tank in PLC) for two values of $k$ : $k = 0.30$, and $k = 0.35$, with step variation of the load resistance to emulate the EV battery charging process. The simulated circuit is almost the same as in Fig. 4, with only $V_p$ being replaced by a inverter with an appropriate DC voltage source input corresponding to $V_p$, and $R_0$ being replaced by a rectifier having a DC filter capacitor of 50 $\mu$F and a variable battery resistance $R_{Bat} = V_{Bat}/I_{Bat}$ at its output. Simulation parameters are given in Table III. The base frequency is $f_{base} = 50$ kHz. The input voltage $V_p$ varies based on the value of $k$, as per the equation $V_p = (\sqrt{8}/\pi) \times kV_{Bat}\sqrt{L_p/L_s}$. Based on the designed parameter values, the frequency response characteristics of the circuit in Fig. 4, which is the fundamental harmonic equivalent circuit of the proposed topology, is shown in Fig. 6 for varying load values at k = 0.3. The plots show that constant current and voltage gain characteristics are obtained at the frequencies corresponding to $\omega_{0cc}$ and $\omega_{0cv}$ respectively. The system input phase angle is also zero at the CC and CV mode frequencies. Simulation results are shown in Fig. 7 and Table IV.

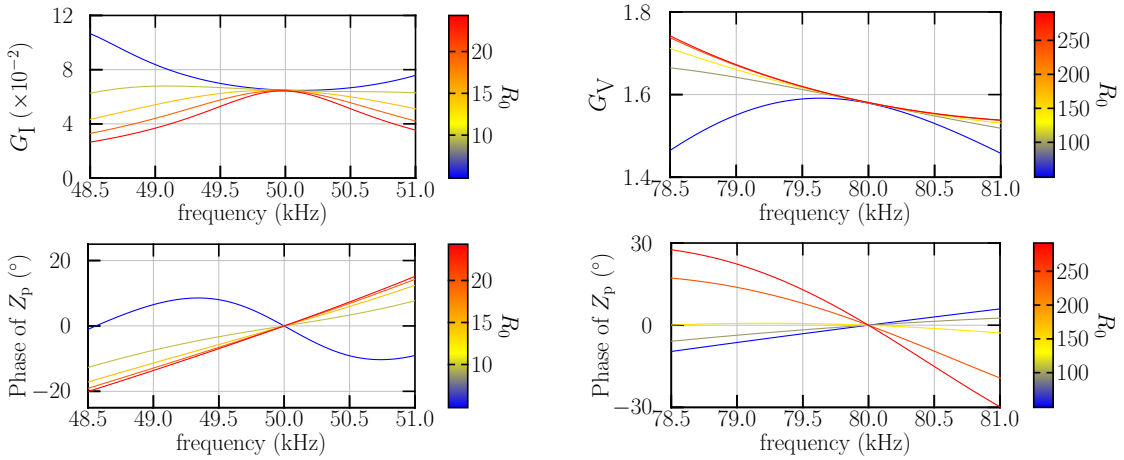


Fig. 6: (a) Transconductance gain and input phase angle at and around $\omega_{0cc}$; (b) Voltage gain and input phase angle at and around $\omega_{0cv}$. The characteristics are shown for the appropriate load ranges for the CC ($R_0 \leq R_{crit}$) and CV modes ($R_0 > R_{crit}$) respectively.

Table IV: Simulation results – output voltage $V_o$, current $I_o$ and input phase angle at each load step

| $R_0$ ($\Omega$) | | 12 | 15 | 18 | 21 | 24 | 27 | 30 | 36 | 42 | 48 | 54 | 60 |
|---|---|---|---|---|---|---|---|---|---|---|---|---|---|
| $V_o$ (V) | $k = 0.30$ | 119.20 | 148.73 | 178.12 | 207.36 | 236.45 | 265.37 | 294.11 | 299.38 | 299.47 | 299.53 | 299.59 | 299.63 |
| | $k = 0.35$ | 119.30 | 148.90 | 178.38 | 207.73 | 236.94 | 265.99 | 294.88 | 299.51 | 299.58 | 299.64 | 299.68 | 299.72 |
| $I_o$ (A) | $k = 0.30$ | 9.93 | 9.92 | 9.90 | 9.87 | 9.85 | 9.83 | 9.80 | 8.32 | 7.13 | 6.24 | 5.55 | 4.99 |
| | $k = 0.35$ | 9.94 | 9.93 | 9.91 | 9.89 | 9.87 | 9.85 | 9.83 | 8.32 | 7.13 | 6.24 | 5.55 | 5.00 |
| $\theta_p$ (°) | $k = 0.30$ | 1.98 | 2.85 | 3.66 | 4.43 | 5.18 | 5.91 | 6.63 | -4.86 | -5.68 | -6.49 | -7.29 | -8.10 |
| | $k = 0.35$ | 1.67 | 2.61 | 3.46 | 4.27 | 5.05 | 5.81 | 6.55 | -4.97 | -5.80 | -6.63 | -7.45 | -8.27 |

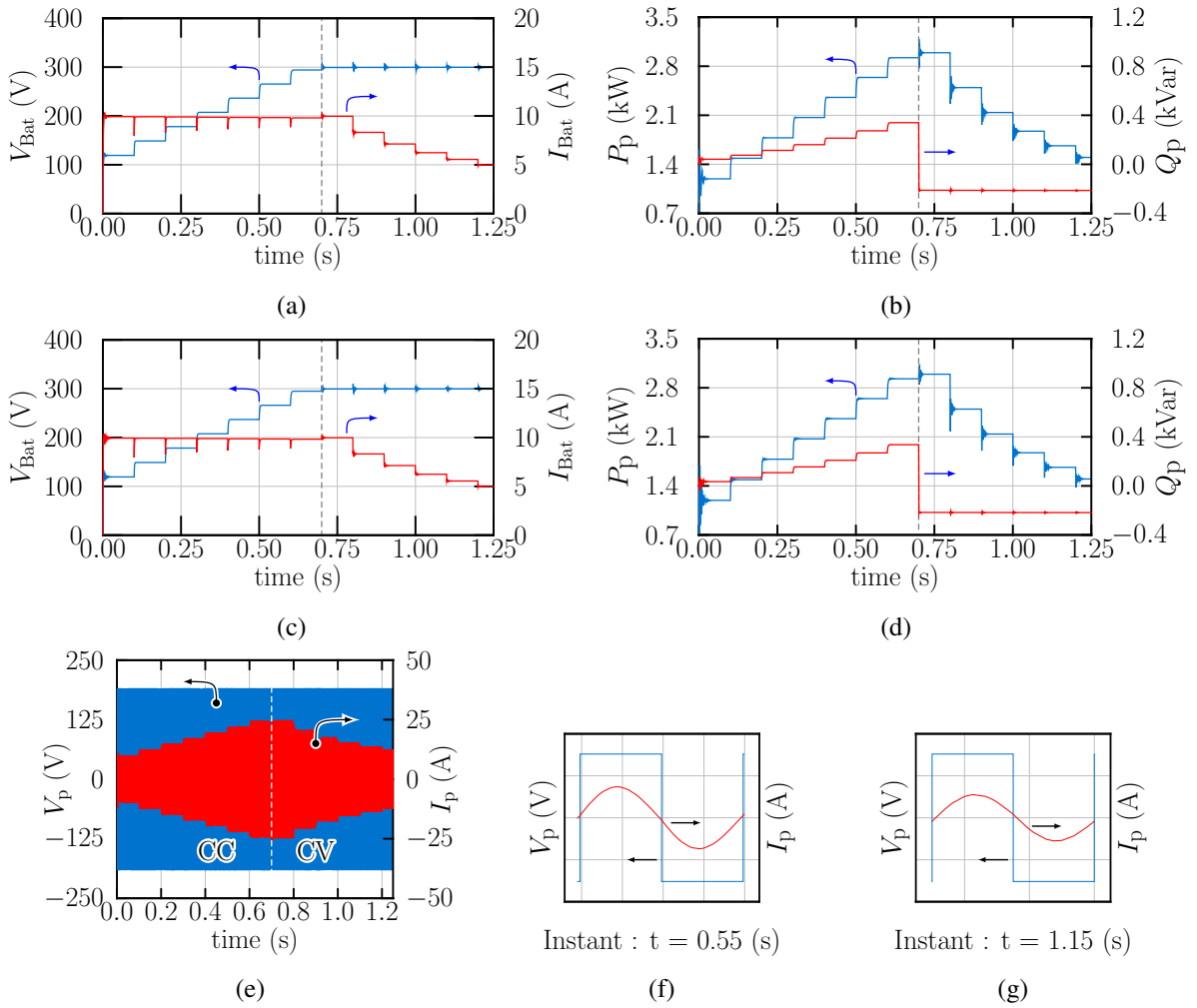


Fig. 7: Simulation results showing output voltage $V_{\text{Bat}}$ and current $I_{\text{Bat}}$ across load $R_0$, along with input side active and reactive power $P_{\text{p}}$ and $Q_{\text{p}}$ respectively. The plots for $k = 0.3$ are (a) $V_{\text{Bat}}$ and $I_{\text{Bat}}$, and (b) $P_{\text{p}}$ and $Q_{\text{p}}$; and for $k = 0.35$ are (c) $V_{\text{Bat}}$ and $I_{\text{Bat}}$, and (d) $P_{\text{p}}$ and $Q_{\text{p}}$. Plots of $V_{\text{p}}$ and $I_{\text{p}}$ for $k = 0.30$ are given in Fig. 7e. $V_{\text{p}}$ and $I_{\text{p}}$ for one switching cycle are also shown (for $k = 0.30$) in Fig. 7f (CC mode) and Fig. 7g (CV mode).

The results show that a constant current of 10 A in the CC mode, and voltage of 300 V in the CV mode is achieved for both $k = 0.30$ and $k = 0.35$ as given in Table IV, with very minor variations in the output current and voltage (due to stray resistances purposefully included in simulation). The spikes observed in all the plots are due to the step changes in the load which will not be present in a realistic system having the battery of the EV. The primary input phase angle $\theta_p$ in Table IV is small (though not negligible) throughout the CC and CV modes, irrespective of $k$. This is also evident in Fig. 7f and Fig. 7g, which show the plots of $V_{\text{p}}$ and $I_{\text{p}}$ for one instant during the CC and CV modes respectively for $k = 0.30$. The reason for this is the presence of the filter capacitor at the rectifier output. As a result, non-zero reactive power $Q_{\text{p}}$ is drawn, which is not desired as the reactive power requirement of the circuit in Fig. 4 is $\simeq 0$. This occurrence can be eliminated by adjusting both $\omega_{0\text{cc}}$ and $\omega_{0\text{cv}}$ as per requirement so that $\theta_p$ can be nullified during the whole operation. Thus closed loop control of the system is required to counter the rectifier action and achieve ZPA. The phase difference can also be utilized to make the inverter output current $I_{\text{p}}$ slightly lagging so as to enable soft switching (zero voltage switching or ZVS) operation. The output plots given in Fig. 7a and Fig. 7c indicate that there is a steady transfer of active power as per load requirement for both the coupling conditions and modes. It can also be seen that the CC to CV mode transition (at $t = 0.7$ s, wherein the operating frequency changes from $\omega_{0\text{cc}}$ to $\omega_{0\text{cv}}$) is smooth and the fluctuations are not drastic. These findings validate the fulfillment of the desired targets in the proposed

topology. Moreover, the simulated performance is also indicative of the robustness of the proposed topology as it can negotiate misalignment between the coils (which causes variations in the coupling coefficient) and provide the desired output current or voltage.

## Conclusions

In this paper a dual output contactless charger with minimal dependence on both coil coupling coefficient and load variation has been proposed. This is achieved by utilizing passive network stages in the WBC which are used to reconfigure the circuit by employing resonance as per requirement. Proper analysis has been provided to describe the process of developing the proposed topology. Thereafter, in-depth explanation of the design methodology of the topology has also been given. Simulation results are then presented in detail to validate the effectiveness of the topology, wherein near ZPA enabled CC and CV outputs are obtained for a range of values of $k$ at load and coupling independent frequencies.

## References


[1] Vu V.B., Tran D.H. and Choi W.: Implementation of the constant current and constant voltage charge of inductive power transfer systems with the double-sided LCC compensation topology for electric vehicle battery charge applications, IEEE Transactions on Power Electronics Vol 33 no 9, pp.7398-7410.

[2] Zhang W., Wong S.C., Chi K.T. and Chen Q.: Analysis and comparison of secondary series-and parallel-compensated inductive power transfer systems operating for optimal efficiency and load-independent voltage-transfer ratio, IEEE Transactions on Power Electronics Vol 29 no 6, pp.2979-2990.

[3] Huang Z., Wong S.C. and Chi K.T.: Design of a single-stage inductive-power-transfer converter for efficient EV battery charging, IEEE Transactions on Vehicular Technology Vol 66 no 7, pp.5808-5821.

[4] Cai C., Wang J., Fang Z., Zhang P., Hu M., Zhang J., Li L. and Lin Z.: Design and optimization of load-independent magnetic resonant wireless charging system for electric vehicles, IEEE Access Vol 6, pp.17264-17274.

[5] Chen Y., Zhang H., Park S.J. and Kim D.H.: A switching hybrid LCC-S compensation topology for constant current/voltage EV wireless charging, IEEE Access Vol 7, pp.133924-133935.

[6] Qu X., Han H., Wong S.C., Chi K.T. and Chen W.: Hybrid IPT topologies with constant current or constant voltage output for battery charging applications, IEEE Transactions on Power Electronics Vol 30 no 11, pp.6329-6337.

[7] Zhang W. and Mi C.C., 2015.: Compensation topologies of high-power wireless power transfer systems, IEEE Transactions on Vehicular Technology Vol 65 no 6, pp.4768-4778.

[8] Wang C.S., Stielau O.H., and Covic G.A., 2005.: Design considerations for a contactless electric vehicle battery charger, IEEE Transactions on Industrial Electronics Vol 52 no 5, pp.1308-1314.